Int. J. Electrochem. Sci., 14 **(2019)** 999 – 1008, doi: 10.20964/2019.01.69

International Journal of
ELECTROCHEMICAL
SCIENCE
www.electrochemsci.org

Corrosion Inhibition of Carbon Steel by 1-Phenyl-3-Amino-5-Pyrazolone in H_2SO_4 Solution

Yan Zhang[1], *Yongfeng Cheng*[1], *Fubin Ma*[2], *Kun Cao*[3,*]

[1] China Electric Power Research Institute, Beijing, 100192, China
[2] Institute of Oceanology, Chinese Academy of Sciences, Qingdao, 266000, China
[3] Department of Chemistry & Chemical Engineering, Neijiang Normal University, Neijiang, Sichuan, 641112, PR China
[*]E-mail: kevin_cao0811@126.com

Received: 27 August 2018 / *Accepted:* 10 October 2018 / *Published:* 30 November 2018

Corrosion inhibition efficiency of 1-phenyl-3-amino-5-pyrazolone (PAP) on mild steel in 0.5 mol/L sulfuric acid (H_2SO_4) solution was investigated by weight loss measurements, potentiodynamic polarization technique, electrochemical impedance spectroscopy (EIS). Measurement of the weight loss shows an inhibition efficiency of about 58.9% in the presence of 0.05 mmol/L PAP, which increases to about 93% at a PAP concentration of 1 mmol/L. Potentiodynamic polarization measurements and EIS reveal that PAP is an excellent corrosion inhibitor of mild steel in 0.5 mol/L H_2SO_4 solution with an efficiency higher than 98% at 1 mmol/L at 298 K. The inhibitor adsorption on the steel surface follows the Langmuir adsorption isotherm.

Keywords: Pyrazolone; mild steel; electrochemical impedance spectroscopy; corrosion inhibitor.

1. INTRODUCTION

Carbon steel plays an important role in industrial infrastructure and facilities because of its excellent thermal conductivity, ductility, and good cost-effectiveness ratio. In the chemical industry, a huge amount of H_2SO_4 is being used for removal of undesired scales and rust, which causes significant metal loss [1,2]. Corrosion inhibitors are always added in acid solution for minimizing acid media attack on metal [3,4]. First, inorganic salts, such as nitrite and phosphonates, are selected as corrosion inhibitors. The main disadvantage of inorganic inhibitors is their toxicity [5–7]. Nowadays, natural extracts and organic chemicals are used as corrosion inhibitors because of heteroatoms and unsaturated bonds that are present in their structures [8–15].

Paulina et al. [16] synthesized two ionic liquids as corrosion inhibitors for API–X52 steel in HCl

solution, which revealed that the two inhibitors worked as mixed-type inhibitors. Their anticorrosion performance depends on temperature, immersion time, and concentration and is remarkably effective at 40 °C, which was attributed to the high thermal stability of the methyl sulfate anions. Hussein et al. [17] synthesized a thiadiazol derivative containing an imino group, which protects the mild steel by forming a protective coating layer. The film became weak at higher temperature. Allal et al. [18] theoretically studied some thiophene derivatives as aluminum corrosion inhibitors. Quantum chemical calculations and molecular dynamics simulations showed that the inhibitors adsorbed on the Al(111) surface, and the calculated inhibition efficiency was overall in good agreement with the experimental value. Sayed et al. [19] synthesized, characterized, and studied the potential of some pyrazole, pyrazolone, and enaminonitrile pyrazole derivatives in anticorrosion and antimicrobial applications.. The results showed that these inhibitors are highly efficient as corrosion inhibitors for the prevention of copper dissolution in NH_4OH solution at pH 9 and have higher antibacterial activities than conventional bactericide agents. The results of the antimicrobial activities and the corrosion inhibition tendencies of these compounds were correlated to their chemical structures.

Our previous work has shown that 1-phenyl-3-methyl-5-pyrazolone is an excellent corrosion inhibitor for mild steel in hydrochloric acid solution [20], which proved that pyrazolone derivatives can be used as potential inhibitors. In this work, we used a similar compound, the pyrazolone derivative 1-phenyl-3-amino-5-pyrazolone (PAP), as corrosion inhibitor. PAP is commonly used as pharmaceutical intermediate, possesses nitrogen and oxygen in its molecular structure, and is water soluble.

2. EXPERIMENTAL SECTION

1-Phenyl-3-amino-5-pyrazolone (PAP) was supplied by Alfa Aesar. As corrosion medium, 0.5 mol/L sulfuric acid solution was used, and the inhibitor PAP was dissolved in this medium to reach concentrations between 0.05 and 1 mmol/L.

The carbon steel was mechanically cut into pieces with side lengths of 5.0 × 2.5 × 0.4 cm for weight loss test and cubes with a side length of 0.1 cm for electrode fabrication. All of the samples were abraded using 200# to 1200# sandpaper, then successively washed with deionized water and ethanol, and dried with nitrogen.

2.1 Electrochemical experiments

Electrochemical experiments were performed in a three-electrode system with a saturated calomel reference electrode and platinum counter electrode using a PARSTAT 2273 electrochemical workstation. Carbon steel was sealed with epoxy resin, exposing a surface of 1 cm^2 as working electrode. Measurements were performed at 298 K.

EIS measurements were carried out in a frequency range of 100 kHz to 10 mHz with an AC voltage amplitude of 10 mV at the open circuit potential (OCP). The inhibition efficiency was calculated by eq 1:

$$\eta_R\% = \frac{R_{ct} - R_{0,ct}}{R_{ct}} \times 100 \quad (1)$$

where R_{ct} and $R_{0,ct}$ represent the resistance of charge transfer in presence and absence of the inhibitor, respectively.

For potentiodynamic polarization experiments, the potential was scanned from –250 to +250 mV vs OCP at a scan rate of 1 mVs^{-1}. The inhibition efficiency was calculated by eq 2:

$$\eta_i\% = \frac{i_{0,corr} - i_{corr}}{i_{0,corr}} \times 100 \quad (2)$$

where i_{corr} and $i_{0,corr}$ are the corrosion current density of mild steel with and without the inhibitor in 0.5 mol/L sulfuric acid solution, respectively.

2.2 Weight loss experiment

Carbon steel samples were fully immersed immersed in the 0.5mol/L sulfuric acid solution for 3 h at 298 K. Samples were weighted before and after 3 h immersion, and the weight differences were calculated.

The inhibition efficiency (η_W%) was evaluated by following equation using weight loss data:

$$\eta_W\% = \frac{C_{R,0} - C_R}{C_{R,0}} \times 100 \quad (3)$$

where $C_{R,0}$ and C_R are the corrosion rate of carbon steel in 0.5 mol/L sulfuric acid solution without and with the inhibitor, respectively. The mean corrosion rate (C_R, mg cm^{-2} h^{-1}) was calculated using the following equation:

$$C_R = \frac{87.6W}{AtD} \quad (4)$$

where W is the weight loss of mild steel (mg), A the area of the working electrode (cm^2), t is the exposure time (h), and D the density of carbon steel (7.85 g/cm^3).

2.3 Surface analysis

The surface morphology of carbon steel was studied in the absence and presence of PAP by scanning electron microscopy (SEM) using the SEM instrument KYKY2800B at 1000× magnification. The specimens were analyzed after an immersion time of 3 h in the absence and presence of the inhibitor at a concentration of 1 mmol/L.

3. RESULTS AND DISCUSSION

3.1 Electrochemical impedance spectroscopy

Electrochemical impedance spectroscopy (EIS) was performed to analyze the adsorptive

interaction of the synthesized organic compound at the metal/solution interface. Fig. 1 shows the impedance responses of carbon steel in the absence and presence of PAP. The impedance spectra clearly exhibit a large capacitive loop. In the presence of PAP, compared with blank solution, this shape is maintained throughout all tested concentrations, indicating that almost no change in the corrosion mechanism occurs due to the inhibitor addition. The large capacitive loop indicates that the corrosion of steel is mainly controlled by a charge transfer process, which is usually related to the charge transfer of the corrosion process and the double layer behavior [21]. The capacitive loops of the semi-circles are not ideal but depressed with centers below the real axis, which is typical of solid electrodes that show frequency dispersion. However, the diameter of the semi-circle of the mild steel sample in 0.5 mol/L H_2SO_4 was found to slightly increase as different concentrations of PAP were introduced into the acidic medium. This indicates the corrosion inhibition capacity of PAP for carbon steel in the acidic environment.

The impedance parameters calculated from these plots by fitting the equivalent circuit (as shown in Fig. 2) are given in Table 1. The equivalent circuit consists of a solution resistance (R_s), a charge transfer resistance (R_{ct}), and an electrical double layer capacitance (C_{dl}). The double layer at the interface did not correspond to an ideal capacitor; thus, a constant phase element was introduced to replace the double layer. The impedance of the CPE and the double layer capacitances C_{dl} were expressed as eqs 5 and 6 [22] where Y_0 is a proportionality coefficient, $j^2 = -1$ is an imaginary number, ω is the angular frequency, and n is the phase shift. The phase shift corresponds to the degree of surface inhomogeneity [23,24]. The behavior of CPE varies with the value of n: when n = 0 and Y_0 = R, CPE behaves as a resistance; when n = 1 and Y_0 = C, CPE represents a capacitance; when n = –1 and Y_0 = L, CPE is an inductance; and when n = 0.5 and Y_0 = W, CPE is a Warburg impedance.

$$Q_{CPE} = Y_0^{-1}\left(j\omega\right)^{-n} \quad (5)$$

$$C_{dl} = Y_0\left(\omega_m\right)^{n-1} \quad (6)$$

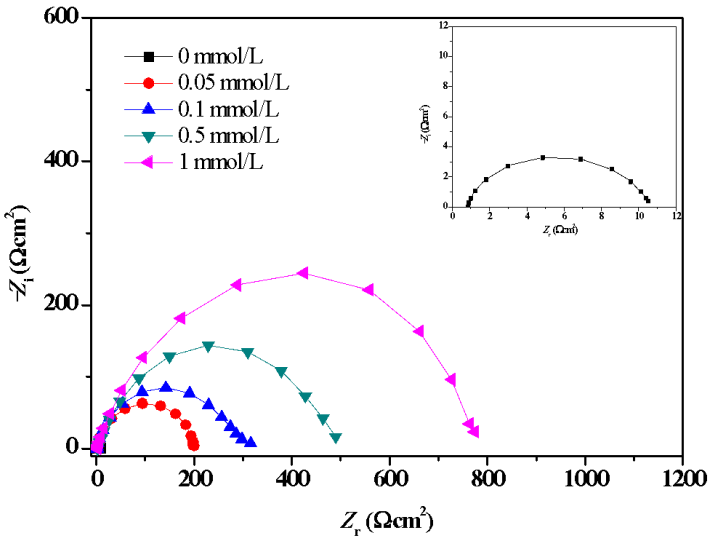

Figure 1. EIS plots of mild steel in 0.5 mol/L H_2SO_4 solution with various concentrations of PAP.

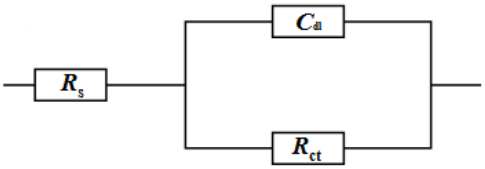

Figure 2. Equivalent circuit of the Nyquist plot.

Table 1. Impedance data of mild steel in 0.5 mol/L H_2SO_4 solution with different concentrations of PAP

	C (mmol/L)	R_s ($\Omega \cdot cm^2$)	C_{dl} ($\mu F \cdot cm^{-2}$)	R_{ct} ($\Omega \cdot cm^2$)	η_R (%)
Blank	0	0.841	9.694	10.24	–
PAP	0.05	1.351	421.4	207.8	95.1
	0.1	1.297	414.1	297.6	96.6
	0.5	1.532	233.0	496.8	97.9
	1	1.702	196.3	786.2	98.7

In the presence of the inhibitor, R_{ct} increased and C_{dl} decreased. This decrease in the C_{dl} values occurs due to the decrease in the local dielectric constant and/or an increase in the thickness of the electrical double layer, which reveals that the inhibitor molecules adsorb at the metal/solution interface [25].

The anticorrosion performance of PAP was also compared with that of other organic inhibitors reported previously. The results are presented in Table 2, revealing that PAP shows a comparable or even better anticorrosion performance than the previously reported organic inhibitors.

Table 2. Comparison of the anticorrosion performance of PAP and other organic inhibitors

Inhibitors	Electrolyte solution	Optimum concentration	Inhibition efficiency (EIS)	Reference
PBI[a]	1 M HCl	2 mmol/L	82.1%	[1]
SB[b]	1 M HCl	1 mmol/L	89.5%	[3]
BMN-2[c]	1 M HCl	150 mg/L	98.5%	[23]
MDDAB[d]	1 M HCl	0.1 mmol/L	95.8%	[26]
2-PCN[e]	0.1 M HCl	10 mmol/L	95.6%	[27]
Rabeprazole sulfide[f]	0.5 M H_2SO_4	1 mmol/L	95.9%	[28]
Bis(coumarin) compounds[g]	0.5 M H_2SO_4	150 ppm	93.1%	[29]
DAP[h]	0.5 M H_2SO_4	10 mmol/L	89.8%	[21]
PMP[i]	1 M HCl	1 mmol/L	97.2%	[20]
PAP	0.5 M H_2SO_4	1 mmol/L	98.7%	This work

[a] 2-(4-pyridyl)-benzimidazole.
[b] (E E)-N,N'-dibenzo [b,d]thiene-2,8-diylbis [1-(thiophen-2-yl)methanimine].
[c] 2-(4-dimethylamino) benzylidine malononitrile.
[d] N-(2-(2-mercaptoacetoxy)ethyl)-N,N-dimethyl dodecan-1-aminium bromide.
[e] 2-pyridinecarbonitrile.

[f] 2- [[4-(3-methoxypropoxy)-3-methylpyridine-2-yl]-methylthio]-1H-benzimidazole.
[g] 7,7'-(naphthalene-2,6-diylbis(methylene))bis(oxy)bis(4-methyl-2H-chromen-2-one).
[h] 2,4-diaminopyrimidine.
[i] 1-phenyl-3-methyl-5-pyrazolone.

3.2 Polarization curve

Potentiodynamic polarization curves for carbon steel in 0.5 mol/L H_2SO_4 with addition of inhibitor at various concentrations (0-1 mmol/L) are shown in Fig. 3. Electrochemical parameters such as corrosion potential (E_{corr}), corrosion current density (i_{corr}), corrosion inhibition efficiency (η_i), anodic Tafel slope (β_a), and cathodic Tafel slope (β_c), as listed in Table 3, were obtained by extrapolating the Tafel plots. As seen in the potentiodynamic polarization curves, inhibitor addition affects both anodic metal dissolution and cathodic hydrogen evolution reactions, which results in the decrease of i_{corr}. The corrosion potential (E_{corr}) values did not shift more than 85 mV with respect to the corrosion potential of the blank solution, which suggests that the inhibitor acts as a mixed-type inhibitor [26,30]. The cathodic (β_c) and anodic Tafel slopes (β_a) barely changed with the inhibitor concentration, which reveals that the inhibitor effectively inhibits the hydrogen evolution reaction. on the cathode and slows the dissolution rate of carbon steel. This proves that the inhibitor adsorbed onto the carbon steel surface and formed a film that hindered the active sites [31,32].

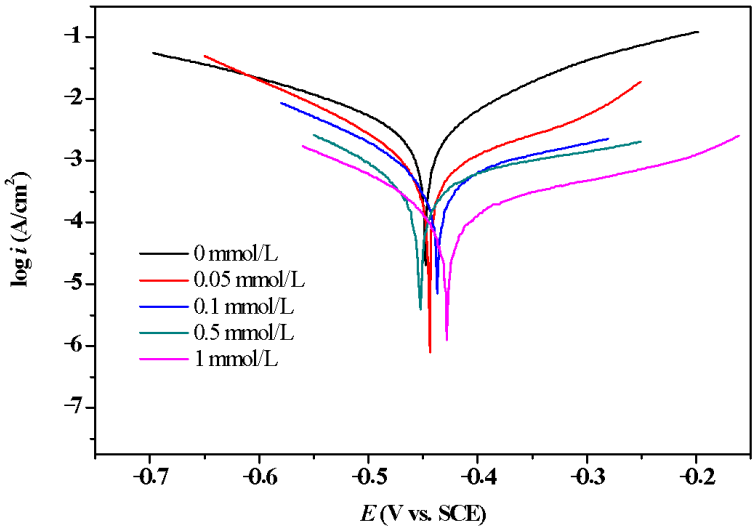

Figure 3. Polarization curves of mild steel in 0.5 mol/L H_2SO_4 solution with different PAP concentrations.

Table 3. Polarization parameters and corresponding inhibition efficiencies for the corrosion of mild steel in 0.5 mol/L H_2SO_4 solution with different PAP concentrations.

	C (mmol/L)	$-E_{corr}$ (mV/SCE)	i_{corr} (μA·cm^{-2})	$-\beta_c$ (mV·dec^{-1})	β_a (mV·dec^{-1})	η_i (%)
Blank	0	0.449	251.2	178	132	
PAP	0.05	0.446	25.12	170	151	90.0

0.1	0.437	15.85	168	165	93.7
0.5	0.465	6.312	161	133	97.5
1	0.429	3.981	170	135	98.4

3.3 Weight loss measurements

The effect of the inhibitor concentration is presented in Fig. 4, which shows that the corrosion rate remarkably decreased and the inhibition efficiency (η_W%) increased with the increase in the inhibitor concentration. Very good η_W% values (98.4%) were obtained at the optimum PAP concentration of 1 mmol/L, which is in good agreement with the η% values obtained from EIS and the polarization curves in 0.5 mol/L sulfuric acid solution.

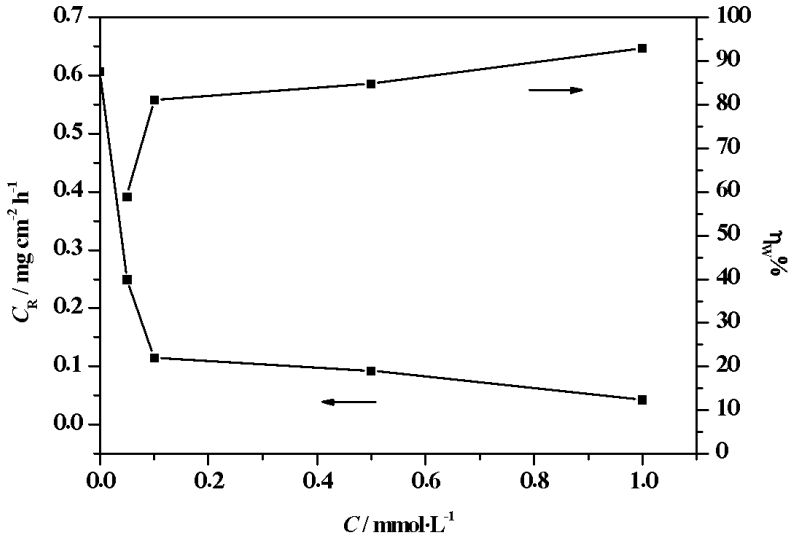

Figure 4. Results of the weight loss experiment.

3.4 Adsorption isotherm

Some supportive information about the mechanism of corrosion inhibition can be obtained from studying the adsorption isotherm. To obtain the isotherm, fractional surface coverages (θ) were determined as a function of the inhibitor concentration. The θ values can be easily calculated from the weight loss measurements. For PAP, the plots of C/θ vs C exhibit straight lines with slopes close to 1, and the linear correlation coefficients were also close to 1 (R^2 = 0.999; Fig. 5), indicating that the adsorption of PAP on the mild steel surface fits well to the Langmuir adsorption isotherm:

$$\frac{C}{\theta} = \frac{1}{K_{ads}} + C \quad ..(7)$$

where K_{ads} is the equilibrium constant of the adsorption/desorption process, and C_{inh} is the inhibitor concentration in the electrolyte, which is related to the standard free energy of adsorption (ΔG_{ads}) according to eq 8. The K_{ads} value of 1.35×10^4 mol^{-1} demonstrates that a high proportion of PAP

adsorbs onto the carbon steel surface. The ΔG_{ads} value was calculated as –33.523 kJ/mol [27,33–42].

$$\Delta G_{ads} = -RT \ln\left(55.5 K_{ads}\right) \quad ..(8)$$

The negative value of ΔG_{ads} indicates that the inhibitor adsorption on the steel surface is spontaneous. Generally, the ΔG_{ads} value is less than –20 kJ/mol and close to –40 kJ/mol, which suggests that a physisorption process (induced by electrostatic interactions between the inhibitor and the charged metal surface) as well as a chemisorption process (charge sharing and transfer from the organic molecules to the metal surface to form a coordinate bond) are involved in the adsorption process [28,43,44].

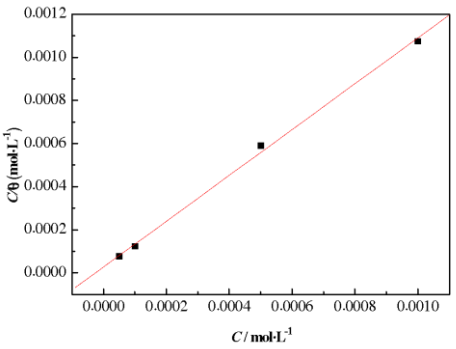

Figure 5. Adsorption isotherm for PAP on the surface of mild steel in 0.5 mol/L H_2SO_4 solution.

3.5 Surface analyses

Images of the carbon steel surface exposed to a 0.5 mol/L H_2SO_4 solution with and without PAP after 3 h were taken by SEM (Fig. 6). Fig. 6a clearly shows that the surface is severely damaged in the inhibitor-free region due to metal dissolution in acidic media. The metal surface was very rough and exhibited deep pits. In contrast, the appearance of the steel surface was different after 3 h immersion in acidic medium containing 1 mmol/L PAP. It can be seen from Fig. 6b that the surface was smoother and had less pits.

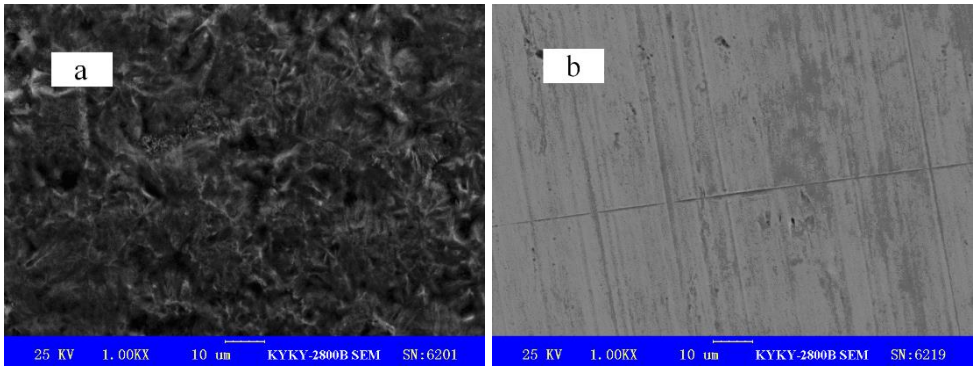

Figure 6. SEM images of the steel surfaces with and without inhibitor: (a) without inhibitor; (b) with 1 mmol/L PAP.

4. CONCLUSION

PAP exhibits a good inhibition performance in 0.5 mol/L H_2SO_4 solution at room temperature. Its efficacy increases with increasing inhibitor concentration and reaches maximum values of 98.7% (determined by EIS) and 98.4% (determined from potentiodynamic polarization curves) at the optimum concentration of 1 mmol/L. Electrochemical tests indicate that PAP acts mainly as a mixed-type inhibitor by an adsorption process. The adsorption of PAP onto the surface of carbon steel obeys the Langmuir adsorption isotherm, occurs spontaneously, and proceeds according to a combined mechanism of chemisorption and physisorption.

ACKNOWLEDGMENTS
The author gratefully acknowledges the support of Science and Technology Project of State Grid Corporation of China (GCB17201600152), National Nature Science Foundation of China (51708541), Key Founding of Sichuan Province Education Department (17ZA0220), Doctor Founding of Neijiang Normal University (No. 15B13), and the Opening Foundation of Key Laboratory of Fruit Waste Treatment and Resource Recycling of the Sichuan Province College (KF17004).

References

1. F. Zhang, Y. Tang, Z. Cao, W. Jing, Z. Wu and Y. Chen, *Corros. Sci.,* 61 (2012) 1.
2. M. J. Bahrami, S. M. A. Hosseini and P. Pilvar, *Corros. Sci.,* 52 (2010) 2793.
3. D. Daoud, T. Douadi, H. Hamani, S. Chafaa and M. Al-Noaimi, *Corros. Sci.*, 94 (2015) 21.
4. E. Gutierrez, J. A. Rodriguez, J. Cruz-Borbolla, J. G. Alvarado-Rodríguez and P. Thangarasu, *Corros. Sci.*, 108 (2016) 23.
5. W. H. Li, Q. He, C. L. Pei and B. R. Hou, *Electrochim. Acta*, 52 (2007) 6386.
6. M. Rohwerder and A. Michalik, *Electrochim. Acta,* 53 (2007) 1300.
7. K. Khaled, *Electrochim. Acta,* 48 (2003) 2493.
8. H. R. Obayes, A. A. Al-Amiery, G. H. Alwan, T. A. Abdullah, A. A. H. Kadhum and A. B. Mohamad, *J. Mol. Struct.*, 1138 (2017) 27.
9. Y. J. Qiang, S. T. Zhang, L. Guo, X. W. Zheng, B. Xiang and S. J. Chen, *Corros. Sci.*, 119 (2017) 68.
10. M. E. Belghiti, Y. Karzazi, A. Dafali, B. Hammouti, F. Bentiss, I. B. Obot, I. Bahadur and E. E. Ebenso, *J. Mol. Liq.*, 218 (2016) 281.
11. M. E. Belghiti, Y. Karzazi, A. Dafali, I. B. Obot, E. E. Ebenso, K. M. Emran, I. Bahadur, B. Hammouti and F. Bentiss, *J. Mol. Liq.*, 216 (2016) 874.
12. L. Guo, S. H. Zhu, S. T. Zhang, Q. He and W. H. Li, *Corros. Sci.*, 87 (2014) 366.
13. P. Han, C. F. Chen, H. B. Yu, Y. Z. Xu and Y. J. Zheng, *Corros. Sci.*, 112 (2016) 128.
14. C. Zhang, H. B. Duan and J. M. Zhao, *Corros. Sci.*, 112 (2016) 160.
15. M. Al-Sabagh, N. M. Nasser, E. A. Khamis and T. Mahmoud, *Egypt. J. Petrol.*, 26 (2017) 41.
16. P. Arellanes-Lozada, O. Olivares-Xometl, N. V. Likhanova, I. V. Lijanova, J. R. Vargas-Garcia and R. E. Hernández-Ramirez, *J. Mol. Liq.*, 265 (2018) 151.
17. H. J. Habeeb, H. M. Luaibi, T. A. Abdullah, R. M. Dakhil, A. A. H. Kadhum and A. A. Al-Amiery, *Case Stud. Therm. Eng.*, 12 (2018) 64.
18. H. Allal and Y. B. EmnaZouaoui, *J. Mol. Liq.*, 265 (2018) 668.
19. G. H. Sayed, M. E. Azab, K. E. Anwer, M. A. Raouf and N. A. Negm, *J. Mol. Liq.*, 252 (2018) 329.
20. K. Cao, W. H. Li, L. M. Yu and B. R. Hou, *Int. J. Electrochem. Sci.*, 7 (2012) 806.
21. X. H. Li and X. G. Xie, *J. Taiwan Inst. Chem. Eng.*, 45 (2014) 3033.

22. Z. Y. Cao, Y. M. Tang, H. Cang, J. Q. Xu, G. Lu and W. H. Jing, *Corros. Sci.*, 83 (2014) 292.
23. D. K. Yadav, M. A. Quraishi and B. Maiti, *Corros. Sci.*, 55 (2012) 254.
24. V. V. Torres, V. A. Rayol, M. Magalhaes, G. M. Viana, L. C. S. Aguiar, S. P. Machado, H. Orofino and E. D'Elia, *Corros. Sci.*, 79 (2014) 108.
25. R. Solmaz, G. Kardas, M. Culha, B. Yazici and M. Erbil, *Electrochim. Acta,* 53 (2008) 5941.
26. M. A. Hegazy, A. M. Badawi, S. S. Abd El Rehim and W. M. Kamel, *Corros. Sci.*, 69 (2013) 110.
27. R. Yildiz, A. Doner, T. Dogan and I. Dehri, *Corros. Sci.*, 82 (2014) 125.
28. M. K. Pavithra, T. V. Venkatesha, M. K. Punith Kumar and H. C. Tondan, *Corros. Sci.*, 60 (2012) 104.
29. M. A. El-Raouf, E. A. Khamis, M. T. H. Abou Kana, N. A. Negm, *J. Mol. Liq.*, 255 (2018) 341.
30. S. S. Shivakumar and K. N. Mohanam, *Corros. Sci.*, 13 (2013) 1.
31. R. Solmaz, E. Altunbas and G. Kardas, *Mater. Chem. Phys.*, 125 (2011) 796.
32. A. O. Yuce and G. Kardas, *Corros. Sci.*, 58 (2012) 86.
33. H. Keles, M. Keles, I. Dehri and O. Serindag, *Mater. Chem. Phys.*, 112 (2008) 173.
34. H. Keles, M. Keles, I. Dehri and O. Serindag, *Colloids Surf. A: Physicochem. Eng. Aspects,* 320 (2008) 138.
35. M. A. Amin and M. M. Ibrahim, *Corros. Sci.*, 53 (2011) 873.
36. M. Lebrini, F. Robert, H. Vezin and C. Roos, *Corros. Sci.*, 52 (2010) 3367.
37. M. J. Bahrami, S. M. A. Hosseini and P. Pilvar, *Corros. Sci.,* 52 (2010) 2793.
38. G. Moretti, F. Guidi and G. Grion, *Corros. Sci.*, 46 (2004) 387.
39. I. Ahamad, R. Prasad and M. A. Quraishi, *Corros. Sci.*, 52 (2010) 933.
40. E. A. Noor and A. H. Al-Moubaraki, *Mater. Chem. Phys.*, 110 (2008) 145.
41. M. Ozcan, R. Solmaz, G. Kardas and I. Dehri, *Colloids Surf. A*, 325 (2008) 57.
42. X. Li, S. Deng and H. Fu, *Corros. Sci.*, 53 (2011) 302.
43. H. M. Abd El-Lateef, V. M. Abbasov, L. I. Aliyeva, E. E. Qasimov and I. T. Ismayilow, *Mater. Chem. Phys.*, 142 (2013) 502.
44. I. Jevremovic, M. Singer, S. Nesic and V. Miskovic-Stankovic, *Corros. Sci.*, 77 (2013) 265.